RAA 2014 Vol. **14** No. **3**, 285–298 doi: 10.1088/1674–4527/14/3/003
http://www.raa-journal.org *http://www.iop.org/journals/raa*

Research in Astronomy and Astrophysics

Non-thermal emissions from accreting X-ray binary pulsars *

Jian-Fu Zhang[1], Hui Jin[1] and Ai-Jun Dong[2]

[1] Department of Physics, Tongren University, Tongren 554300, China; *jianfuzhang.yn@gmail.com*
[2] School of Physics, Huazhong University of Science and Technology, Wuhan 430074, China

Received 2013 August 7; accepted 2013 November 11

Abstract We study non-thermal emissions from cascade processes in accreting X-ray binary pulsars. In the framework of the magnetospheric gap model, we consider three photon fields, which are respectively from the polar cap of a pulsar, its surrounding accretion disk and a massive companion star with a circumstellar disk, to shield the gap. The gap-accelerated ultra-relativistic electrons emit high-energy photons via curvature radiation and an inverse Compton scattering process, in which part of these high-energy photons absorbed by interactions with the surrounding photon fields can facilitate the following electromagnetic cascades. We first carry out numerical calculations of the cascade processes in order to obtain the predicted emission spectra. As an example, we subsequently apply this model to reproduce observations of LS I $+61^\circ$ 303. We find that the results can fit observations ranging from hard X-ray to γ-ray bands. In particular, they can explain the spectral cutoff feature at a few GeV. Finally, we suggest that the emissions detected by the *Fermi* Large Area Telescope from X-ray binary pulsars originate in the magnetosphere region of the pulsar.

Key words: stars: binaries — stars: individual (LS I + 61° 303) — radiation mechanisms: non-thermal — gamma rays: theory

1 INTRODUCTION

Up to now, seven X-ray binaries have been detected at GeV and/or TeV γ-rays by the *Fermi* Large Area Telescope (*Fermi* LAT), the AGILE satellite, the High Energy Stereoscopic System (HESS), the Major Atmospheric Gamma Imaging Cherenkov Telescope (MAGIC) and the Very Energetic Radiation Imaging Telescope Array System (VERITAS): LS 5039 (e.g., Aharonian et al. 2005a; Abdo et al. 2009b), LS I $+61^\circ$ 303 (e.g., Albert et al. 2006; Abdo et al. 2009a), PSR B1259–63 (e.g., Aharonian et al. 2005b; Abdo et al. 2011), Cygnus X-1 (e.g., Albert et al. 2007), Cygnus X-3 (e.g., Abdo et al. 2009c; Piano et al. 2012), HESS J0632+057 (e.g., Aharonian et al. 2007), and 1FGL J1018.6–5856 (Ackermann et al. 2012).

Among them, PSR B1259–63 was found to be a massive binary consisting of a stellar companion and a young non-accreting pulsar. Moreover, Cygnus X-1 and Cygnus X-3 were classified as high-mass microquasars with relativistic radio jets. Recently, HESS J0632+057 (Hinton et al. 2009) and

* Supported by the National Natural Science Foundation of China.

1FGL J1018.6–5856 (Ackermann et al. 2012) were pointed out to be new γ-ray binaries. However, due to the fact that the nature of compact objects is still an open question, LS 5039 and LS I + 61° 303 have been the subject of strong arguments, i.e., are they non-accreting pulsar binaries (e.g., Mirabel 2006; Dubus 2006; Dubus et al. 2008; Zabalza et al. 2011; Mirabel 2012), in which multi-wavelength emissions are due to the shocked pulsar wind interacting with a stellar wind from a high-mass companion, or accreting microquasars (e.g., Paredes et al. 2006; Romero et al. 2007; Khangulyan et al. 2008; Zhang et al. 2009; Bosch-Ramon & Khangulyan 2009; Zhang et al. 2010; Yamaguchi & Takahara 2010; Zhang et al. 2011; Zhang & Feng 2011; Yamaguchi & Takahara 2012), in which emissions are from relativistic jets.

We note three sources, LS I + 61° 303, LS 5039 and 1FGL J1018.6-5856, detected by *Fermi* LAT (Abdo et al. 2009a,b; Ackermann et al. 2012) which present a common feature in their spectral shape. The spectra can be well fitted by a power law plus an exponential cutoff, with the cutoff energies at ~ 2.1 GeV (LS 5039), ~ 6.3 GeV (LS I + 61° 303) and ~ 2.5 GeV (1FGL J1018.6-5856). These cutoff features are very similar to those of many pulsars that have been detected by *Fermi* LAT (Abdo et al. 2009b; Nolan et al. 2012). The emission spectrum of those typically isolated pulsars has a hard power law and an exponential cutoff at ~ 2.5 GeV. These spectral cutoff features seem to indicate that these three sources possibly belong to the same category, and have a common origin for their emission which is similar to that of isolated pulsars (Abdo et al. 2009b). In these cases, the emissions arise from the pulsar's magnetospheric region (e.g., Zhang & Li 2009; Abdo et al. 2009b). On the other hand, the analysis of the light curve along different orbital phases shows that there are anti-correlations between the very high-energy emissions detected by HESS, MAGIC and VERITAS and high-energy emissions detected by *Fermi* LAT (Abdo et al. 2009a,b; Ackermann et al. 2012). These anti-correlations indicate that these emissions should originate from different radiative mechanisms, different emitting particles or different emission regions.

In some massive binary systems that contain a pulsar, such as PSR B1259–63, γ-ray emissions are due to the acceleration of particles as a result of the interaction of the wind from a companion star with the energetic pulsar wind. In this case, the pulsar rotates quite fast to produce an energetic pulsar wind. In the other case, the pulsar is not so energetic that the accreting matter from the stellar wind can fall into the pulsar's inner magnetosphere, and reach its surface (e.g., Lipunov et al. 1992; Bednarek 2009a). From an observational point of view, some evidence agreeing with the latter has also been found (see also e.g., Rodriguez & Bodaghee 2008).

These reports motivate us to study emissions from the magnetospheric region of accreting X-ray pulsars. In the framework of the magnetospheric acceleration model (outer gap model) of Cheng & Ruderman (1989, 1991) for an accreting X-ray binary pulsar, we carry out numerical calculations of the emission spectra when cascade processes occur. As an example, we apply this cascade emission model to fit the *Fermi* LAT observations of LS I + 61° 303 for the first time, and find that the results can reproduce observations from X-ray to GeV bands. This paper is organized as follows. In the next section, some key elements of the outer gap model are provided. Details and numerical results of radiation processes of cascades are presented in Section 3. In Section 4, we apply the magnetospheric emission model to the X-ray binary LS I + 61° 303. A brief summary and discussions are presented in the last section.

2 MODEL OF THE MAGNETOSPHERE

The magnetosphere of a pulsar surrounded by a Keplerian accretion disk was originally proposed by Cheng & Ruderman (1989, 1991). When the inner parts of the accretion disk rotate faster than the pulsar itself, i.e., the angular velocities of the disk $\Omega_{\rm d}$ and pulsar Ω satisfy $\Omega_{\rm d} > \Omega$, inertial effects will lead to a separation of charge in the magnetosphere. An entirely empty gap in the plasma develops and it separates regions of the magnetosphere with opposite charge (see Fig. 1, adapted

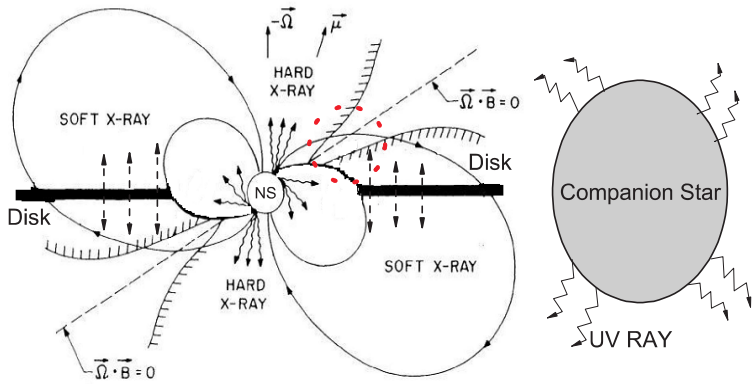

Fig. 1 Geometrical structure of an X-ray pulsar binary system. The three main components are the central neutron star (NS), which emits hard X-rays in its polar cap region, its surrounding conducting Keplerian disk, which produces soft X-ray emissions and a stellar companion, which radiates UV rays. When the spin velocities of the Keplerian disk $\Omega_{\rm d}$ and the NS Ω comply with $\Omega_{\rm d} > \Omega$, an entirely empty plasma gap can be formed. In this gap, the condition of $\boldsymbol{E}\cdot\boldsymbol{B} \neq 0$ is satisfied; as a result, a strong potential drop is established and charged particles can be accelerated to very high energy. These accelerated particles produce cascade processes there. The typical scale of the region where emission occurs (the region inside the dotted circle) is approximated on the order of the inner radius of the accretion disk. This plot was adapted from Cheng & Ruderman (1991).

from Cheng & Ruderman 1991). In this gap, the condition of $\boldsymbol{E}\cdot\boldsymbol{B} \neq 0$ is satisfied, that is electric fields are present along the direction of the magnetic field. These electric fields can establish a strong potential drop and accelerate charged particles. Under a strong shielding condition of the gap, the potential drop can reach the maximum allowable for a static gap,

$$\Delta V_{\rm max} \simeq \frac{B_{\rm s}R^3\Omega_{\rm d}(r_0)}{r_0 c} \simeq 4\times10^{14}\beta^{-5/2}\left(\frac{M_{\rm co}}{M_\odot}\right)^{1/7} R_6^{-4/7}L_{37}^{5/7}B_{12}^{-3/7}\ {\rm V}, \tag{1}$$

where $B_{\rm s}$ is the magnetic field strength of the pulsar's surface, r_0 is the inner radius of the accretion disk, $M_{\rm co}$ is the mass of the compact star, and c is the speed of light. On the right side of Equation (1), the X-ray luminosity L_{37}, pulsar radius R_6 and magnetic field B_{12} are in units of 10^{37} erg s^{-1}, 10^6 cm and 10^{12} G, respectively. The parameter $\beta \equiv 2r_0/r_{\rm A}$ is twice the ratio of the inner accretion disk radius to the Alfvén radius. The Alfvén radius can be determined by the condition that the magnetic energy density of the pulsar field $B^2/8\pi$ equals the kinetic energy density of accreting matter $\rho v(r_A)^2/2$, which results in

$$r_{\rm A} = 3\times10^8\left(\frac{M_{\rm co}}{M_\odot}\right)^{1/7} R_6^{10/7}L_{37}^{-2/7}B_{12}^{4/7}\ {\rm cm}. \tag{2}$$

Through considering the condition that the azimuthal magnetic field induced by the current cannot exceed that of the initial field, the maximum current that can flow through the gap can be written as

$$J_{\rm max} \simeq cB_{\rm s}R^3r_0^2 \simeq 1.5\times10^{24}\beta^{-2}\left(\frac{M_{\rm co}}{M_\odot}\right)^{-2/7} R_6^{1/7}L_{37}^{4/7}B_{12}^{-1/7}\ {\rm esu\ s^{-1}}. \tag{3}$$

Therefore, the total power of current in the gap can be given by

$$P_{\rm gap} \simeq J_{\rm max}\Delta V_{\rm max} \simeq 2\times 10^{36}\beta^{-9/2}\left(\frac{M_{\rm co}}{M_\odot}\right)^{-1/7} R_6^{-3/7} L_{37}^{9/7} B_{12}^{-4/7}\ {\rm erg\ s^{-1}}. \quad (4)$$

In the early magnetospheric model (Cheng & Ruderman 1989, 1991), the gap is filled with hard/soft X-ray photons which arise from the accretion-powered thermal X-rays at the polar caps; alternatively, these thermal X-rays are Compton-degraded when they penetrate the accreting matter flow (e.g., Cheng et al. 1992). In this work, in addition to this photon field, we also consider two other photon sources from the region of an accretion disk (soft X-ray photons from a standard thin accretion disk) and a massive companion (UV photons). This is different from the early emission model (Cheng et al. 1992) in terms of radiation efficiency; the two photon fields we consider will initiate the attenuation and subsequent cascade at higher energy bands. Leptons (electron-positron pairs) and hadrons (protons or ions), which go through the gap region, will be accelerated to ultra-relativistic energies by electric fields, along curved magnetic field lines.

In this paper, we mainly focus on the leptonic scenario. Most photons from curvature emission and those from inverse Compton scattering will change into electron pairs in collisions with surrounding photon fields. The pitch angle of these electron pairs can be given by $\langle\theta\rangle \sim \sin^{-1}(d/s)$. Here d is the distance from the emitting point to the point where pairs are produced, and s is the radius of the local magnetic field line. After considering typical values of d and s, we can obtain that $\langle\theta\rangle$ is on the order of unity. Because the γ-ray can be emitted from any point inside the gap, the distribution of pitch angle for these electron pairs is quite random and uniform. Therefore, equations describing radiation are used to calculate the electromagnetic cascade processes, and are presented in the next section.

3 CASCADE PROCESSES AND NUMERICAL RESULTS

3.1 Production Mechanism of Non-thermal Radiation Spectra

During the process of the matter being accreted from a surrounding companion star onto the central compact star, two strong turbulent/shock regions can be formed; one region can be regarded as the Aflvén region, and the other one is usually considered to be the polar cap region of the pulsar. These regions with disturbance could thermalize and accelerate electrons and protons to generate a power law spectrum which would be preserved in the gap region. (Note that we only concentrate on lepton processes in this study.) Hence, we assume the accelerated electron spectrum in the gap is

$$N(E) = N_0 E^{-\alpha}, \quad (5)$$

where α is a spectral index. The normalization factor N_0 can be obtained by $N_0 = (2-\alpha)\eta P_{\rm gap}/(E_{\rm max}^{2-\alpha} - E_{\rm min}^{2-\alpha})$. The energy conversion efficiency from the gap power to relativistic electrons is parameterized as η, i.e. an effective factor. The electrons accelerated by the electric field in the gap along curved magnetic field lines, whose maximum energy can be limited by loss from curvature radiation, is given by

$$E_{\rm max} = 1.3\times 10^{13}\beta^{-5/8}\left(\frac{M_{\rm co}}{M_\odot}\right)^{1/28} R_6^{-1/7} L_{37}^{5/28} B_{12}^{-3/28} s_8^{1/2} l_8^{-1/4}\ {\rm eV}, \quad (6)$$

where l_8 is the typical size of the gap in units of 10^8 cm and s_8 is a curvature radius of the local magnetic field line in units of 10^8 cm. For simplicity, these two parameters are assumed to be equal to $\sim r_0$ (for a similar assumption, see Cheng et al. 1992; Leung et al. 1993).

These accelerated primary electrons mainly lose their energies by curvature radiation and the inverse Compton scattering (ICS) processes. The photon energy spectrum of curvature radiation is written as

$$F_{\rm cur}(E_\gamma) = \frac{\sqrt{3}{\rm e}^2}{hm_{\rm e}c^2}\int_{E_{\rm min}}^{E_{\rm max}}\frac{EN(E)}{sE_\gamma}\int_{E_\gamma/E_{\rm cur}}^{\infty}K_{5/3}(\zeta)d\zeta dE, \tag{7}$$

where $K_{5/3}(\zeta)$ is the modified Bessel function. The typical energy of curvature radiation is $E_{\rm cur} = (3/2)hcE^3/m_{\rm e}^3c^6s$ and the minimum energy of electrons is set to be $\sim 10\ m_{\rm e}c^2$. The spectral distribution of photons that are affected by ICS is (Blumenthal & Gould 1970)

$$F_{\rm ICS}(E_\gamma) = \frac{3\sigma_{\rm T}c(m_{\rm e}c^2)^2}{4}\int_{E_{\rm min}}^{E_{\rm max}}\frac{N(E)}{E^2}dE\int_{\varepsilon_{\rm min}}^{\varepsilon_{\rm max}}\frac{n(\varepsilon)d\varepsilon}{\varepsilon}Q(q). \tag{8}$$

Here $\sigma_{\rm T}$ is the Thomson cross section, and the function $Q(q)$ is given by $Q(q) = [2q\ln(q) + (1+2q)(1-q) + \frac{(\Pi q)^2(1-q)}{2(1+q)}]$, with $\Pi = 4\varepsilon E/(m_{\rm e}c^2)^2$ and $q = E_\gamma/\Pi E(1-E_\gamma/E)$.

The scattered soft photon density $n(\varepsilon)$ in Equation (8) is $n(\varepsilon) = n_{\rm cap}(\varepsilon) + n_{\rm disk}(\varepsilon) + n_{\rm star}(\varepsilon)$. The photon density $n_{\rm cap}(\varepsilon)$ from the polar cap region is written as

$$n_{\rm cap}(\varepsilon) = \frac{1}{\pi^2(\hbar c)^3}\frac{\varepsilon^2}{\exp(\varepsilon/kT_{\rm cap})-1}\left(\frac{R_{\rm co}}{l}\right)^2, \tag{9}$$

where l is the mean dimension of the emission region (approximated as the gap size). The surface temperature of the polar cap $T_{\rm cap}$ is approximated as $T_{\rm cap} = (L_{\rm x}/\pi R_{\rm cap}^2\sigma_{\rm SB})^{1/4}$, where $\sigma_{\rm SB}$ is the Stefan-Boltzmann constant, the thermal luminosity is $L_{\rm x} \sim G\dot{M}_{\rm acc}M_{\rm co}/R_{\rm co}$ and the radius of the polar cap can be estimated as, by assuming a dipolar structure of the magnetic field, $R_{\rm cap} = (R_{\rm co}/r_{\rm A})^3$. As for the photon density of the accretion disk, we adopt the standard accretion disk (Shakura & Sunyaev 1973), which is optically thick, geometrically thin and flat. In this theory that describes a thin accretion disk, each surface element of the disk is in thermal equilibrium. The surface temperature of the disk follows

$$T_{\rm disk}(r) = \left(\frac{3\dot{M}_{\rm acc}c^6}{8\pi\sigma_{\rm SB}G^2M_{\rm co}^2}\right)^{\frac{1}{4}}\left(\frac{rc^2}{GM_{\rm co}}\right)^{-\frac{3}{4}} \simeq 1.25\times10^6\,\dot{M}_8^{1/4}\,M_{1.4}^{1/4}\,r_8^{-3/4}\ {\rm K}, \tag{10}$$

where $\dot{M}_8$ is the accretion rate in units of $10^{-8}\ M_\odot\ {\rm yr}^{-1}$, $M_{1.4}$ is the mass of the compact star in units of $1.4\ M_\odot$, and r_8 is the disk radius in units of 10^8 cm. Due to the gap being located inside the inner accretion disk, the photon density from the disk is given as (e.g., Frank et al. 2002; Kato et al. 2008)

$$n_{\rm disk}(\varepsilon) = \frac{1}{\pi^2(\hbar c)^3}\frac{\varepsilon^2}{\exp[\varepsilon/kT_{\rm disk}(r)]-1}. \tag{11}$$

Furthermore, we consider $T_{\rm disk}(r) = T_{\rm disk}(r_{\rm o})$ for simplicity. For massive early-type stars such as LS I +61° 303, with a cold circumstellar disk, one has to consider the contribution of the photon field from the stellar disk. The photon density of the stellar disk is given as

$$n_{\rm sd}(\varepsilon) = \frac{1}{\pi^2(\hbar c)^3}\frac{\varepsilon^2}{\exp(\varepsilon/kT_{\rm sd})-1}\left(\frac{r}{R_{\rm orbit}-l}\right)^2, \tag{12}$$

where $T_{\rm sd}$ is the effective temperature of the circumstellar disk. The photon field of the massive companion is

$$n_{\rm star}(\varepsilon) = \frac{1}{\pi^2(\hbar c)^3}\frac{\varepsilon^2}{\exp(\varepsilon/kT_{\rm star})-1}\left(\frac{R_{\rm star}}{R_{\rm orbit}-l}\right)^2, \tag{13}$$

where $R_{\rm star}$ is the radius of the companion star, and $R_{\rm orbit}$ is the orbital radius of the binary system.

Most of the emitted primary photons will be attenuated by the photon fields from the polar cap (Eq. (9)), the inner disk region (Eq. (11)) and the companion star (Eqs. (12) and (13)), producing electron-positron pairs. The surviving primary photon spectrum is modified by

$$F_{\rm sur,p}(E_\gamma) = [F_{\rm cur}(E_\gamma) + F_{\rm ICS}(E_\gamma)]{\rm e}^{-\tau(E_\gamma)}, \tag{14}$$

where $\tau(E_\gamma)$ is the optical depth due to pair production, and is given as (Jauch & Rohrlich 1976)

$$\tau(E_\gamma) = l\int_{\varepsilon_{\rm th}}^{\infty} n(\varepsilon)\sigma_{\rm pair}(\varepsilon, E_\gamma)d\varepsilon. \tag{15}$$

The cross section for pair production is expressed by

$$\sigma_{\rm pair}(\varepsilon, E_\gamma) = \frac{3}{16}\sigma_{\rm T}(1-\lambda^2)\left[2\lambda(\lambda^2-2) + (3-\lambda^4)\ln\left(\frac{1+\lambda}{1-\lambda}\right)\right], \tag{16}$$

with $\lambda = (1 - m_{\rm e}^2c^4/\varepsilon E_\gamma)^{1/2}$. In Equation (15), the threshold energy of pair production is $\varepsilon_{\rm th} = m_{\rm e}^2c^4/E_\gamma$.

The spectral energy distribution of the secondary pair is (Blumenthal & Gould 1970)

$$N_{\rm sec}(E_{\rm sec}) = \frac{dN_{\rm sec}(E_{\rm sec})}{dE_{\rm sec}} = \frac{1}{\dot{E}_{\rm sec}}\int_{E_{\rm sec}}^{E_{\rm sec,max}} \dot{G}(E'_{\rm sec})dE'_{\rm sec}, \tag{17}$$

where

$$\dot{G}(E'_{\rm sec}) = 2\{1-\exp[-\tau(E'_\gamma)]\} \times [F_{\rm cur}(E'_\gamma) + F_{\rm ICS}(E'_\gamma)] \tag{18}$$

with $E'_{\rm sec} \sim 0.5\ E'_\gamma$. The energy loss rate of secondary electrons is the sum of the synchrotron and ICS loss rates, $\dot{E}_{\rm sec}(E_{\rm sec}) = \dot{E}_{\rm sec,syn}(E_{\rm sec}) + \dot{E}_{\rm sec,ICS}(E_{\rm sec})$. The synchrotron loss rate is

$$\dot{E}_{\rm sec,syn}(E_{\rm sec}) = \frac{c\sigma_{\rm T}}{4\pi}\frac{E_{\rm sec}^2}{(m_{\rm e}c^2)^2}B^2, \tag{19}$$

and the ICS loss rate is given by (Bosch-Ramon & Khangulyan 2009)

$$\dot{E}_{\rm sec,ICS}(E_{\rm sec}) = 5.5\times10^{17}\left(\frac{kT}{m_{\rm e}c^2}\right)^3\frac{E_{\rm sec}}{m_{\rm e}c^2}\frac{\ln[1+0.55E_{\rm sec}kT/(m_{\rm e}c^2)^2]}{1+25E_{\rm sec}kT/(m_{\rm e}c^2)^2} \times\left\{1+\frac{1.4E_{\rm sec}kT/(m_{\rm e}c^2)^2}{1+12[E_{\rm sec}kT/(m_{\rm e}c^2)^2]^2}\right\}. \tag{20}$$

These secondary pairs will emit secondary γ-rays via synchrotron radiation and ICS processes (see Eq. (8)). The synchrotron radiation spectrum for an ensemble of secondary pairs is

$$F_{\rm sec,syn}(E_\gamma) = \frac{\sqrt{3}{\rm e}^2}{2\pi\hbar c}\int_{E_{\rm sec,min}}^{E_{\rm sec,max}}\frac{dN_{\rm sec}(E_{\rm sec})}{dE_{\rm sec}}\frac{eB}{m_{\rm e}cE_\gamma}\left(1-\frac{E_\gamma}{E_{\rm sec}}\right)\Theta(\xi)dE_{\rm sec} \tag{21}$$

in a strong magnetic field, where the function $\Theta(\xi)$ is given by (Harding & Preece 1987)

$$\Theta(\xi) = \digamma(\xi) + \xi^3\left(\frac{3E_{\rm sec}}{2m_{\rm e}c^2}\epsilon_{\rm B}\right)^3\left(1-\frac{E_\gamma}{E_{\rm sec}}\right)K_{3/2}(\xi), \tag{22}$$

with $\digamma(\xi) = \xi\int_\xi^\infty K_{5/3}(\zeta)d\zeta$, $\xi = E_\gamma/E_{\rm sec,c}$ and $E_{\rm sec,c} = (3/2)\hbar(eB/m_{\rm e}c)(E_{\rm sec}/m_{\rm e}c^2)^2(1 - E_\gamma/E_{\rm sec})$; $K_{3/2}(\xi)$ is the Bessel function. Here, $\epsilon_{\rm B}$ is defined as $\epsilon_{\rm B} = B/B_{\rm cr}$, and $B_{\rm cr} =$

$m_e^2 c^3/e\hbar \simeq 4.414 \times 10^{13}$ G is a critical magnetic field strength. When using Equation (8) to calculate the secondary ICS spectrum, we consider the contributions of the soft photon $n_{\rm syn}(\varepsilon)$ from the synchrotron emission of secondary pairs, which is approximated as

$$n_{\rm syn}(\varepsilon) = \frac{F_{\rm syn}(E_\gamma)}{l^2 c}. \tag{23}$$

Hence, the total density of seed photons is now $n(\varepsilon) = n_{\rm cap}(\varepsilon) + n_{\rm disc}(\varepsilon) + n_{\rm star}(\varepsilon) + n_{\rm syn}(\varepsilon)$; we find that $n_{\rm syn}(\varepsilon)$ is dominant in terms of our numerical calculations.

These secondary γ-ray spectra will also be further attenuated by surrounding X/UV-rays. The surviving secondary photon spectrum is modified by

$$F_{\rm sur,sec}(E_\gamma) = [F_{\rm sec,syn}(E_\gamma) + F_{\rm sec,ICS}(E_\gamma)]{\rm e}^{-\tau(E_\gamma)}. \tag{24}$$

In Equation (24), when calculating optical depth $\tau(E_\gamma)$, the effects of the synchrotron photon density $n_{\rm syn}(\varepsilon)$ from secondary pairs is also considered. Parts of the absorbed secondary photons are also energetic enough to produce a third generation of pairs, which can also emit a third generation of γ-rays via synchrotron and ICS processes. In turn, these third generation γ-rays will induce the next generation of cascade processes. For these cascade processes, we can repeatedly use Equations (8) and (21) to carry out the calculation procedures. Finally, the total output spectrum of gamma-rays can be expressed by

$$F_{\rm total}(E_\gamma) = \sum_{i=1}^{n} F_{{\rm sur},i}(E_\gamma), \tag{25}$$

where $F_{{\rm sur},i}(E_\gamma)$ is the ith generation of the surviving spectrum, and n indicates the generation number of a cascade.

3.2 Numerical Results

In this section, we will adopt the formulae given in Section 3.1 to calculate cascade processes. We first calculate the optical depth for various photon fields by using Equation (15), before carrying out calculations of radiation spectra. The attenuation factor as a function of photon energies is shown in Figure 2. As shown in this figure, three significant attenuation troughs are presented at γ-ray bands. The hard X-rays from the polar cap affect γ-rays above $\sim$ 100 MeV, and the soft X-rays from the inner accretion disk absorb the photons above $\sim$ 1 GeV, whereas the UV photons from the surrounding massive star interacting with high energy photons are slightly weak, for the current parameters. It should be noted that the attenuation at very high energy bands will become heavier for a massive close binary. These attenuations can also induce the orbital modulation of emissions due to changes in photon densities at different phases (see also Fig. 3). Alternatively, locations of these different attenuation troughs can also be estimated by $E_\gamma \geq m_e^2 c^4/\varepsilon$.

Among all the model parameters, the magnetic field of pulsar B_{12} and accretion rate $\dot{M}_8$ are important. Once provided an accretion rate, one can determine temperatures of the inner disk and polar cap by virtue of related parameters, such as mass of the central compact star and its radius. However, these temperatures are very sensitive to attenuation effects and cascade processes. Moreover, the magnetic field of a pulsar's surface can limit the magnetic field in the gap region by assuming there is a bipolar magnetic field. In Figure 4, we plot the cascade photon spectra up to the fifth generation for a general accreting X-ray binary pulsar; a further cascade is negligible. The model parameters are listed in the caption of the figure.

In Figure 3, the total output spectra (thick solid line) are the sum of the emission spectrum for each individual generation. The primary curvature and ICS photon spectra are indicated by a

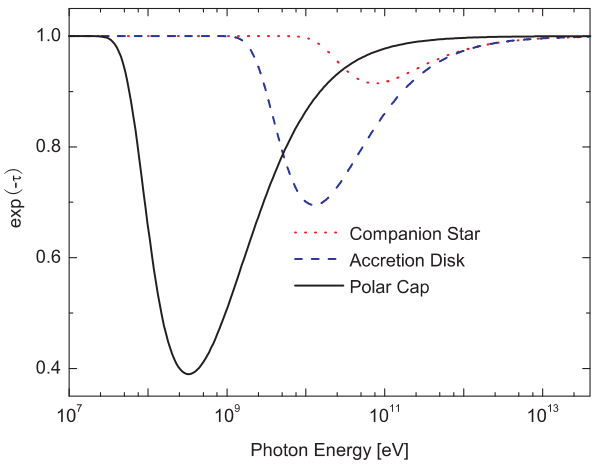

Fig. 2 Attenuation factors due to three photon fields. The accretion rate and the radius of the pulsar are set as $0.1\ \dot{M}_8$ and 10^6 cm, respectively. The other parameters are: the effective temperature of a massive star is 5×10^4 K, the radius of the companion star is $10\ R_\odot$ and the orbital radius of the binary system is 10^{11} cm.

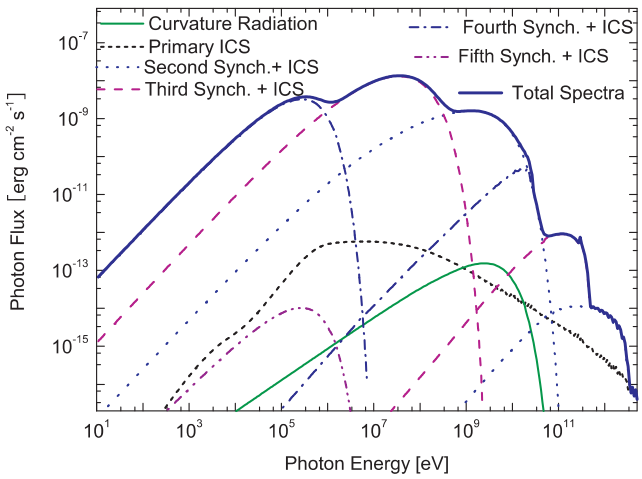

Fig. 3 Emission spectra for a general accreting X-ray binary pulsar. The model parameters are the accretion rate of $0.02\ \dot{M}_8$, effective factor of $\eta = 0.01$, magnetic field of the pulsar's surface of $1\ B_{12}$, orbital distance of 10^{12} cm, pulsar mass of $1.4\ M_\odot$ and spectral index of 2.5. The other parameters are the radius of the companion star of $10\ R_\odot$ and effective temperature of the massive star of 5×10^4 K.

thin solid line and short-dashed line, respectively. Moreover, the second to the fifth generation of synchrotron and ICS spectra are indicated by dotted, dashed, dot-dashed and dot-dot-dashed lines, respectively. The primary curvature and each ICS spectrum, which present low fluxes (small numbers of photons), will not contribute to observational photon flux (including in the TeV domain for current telescopes). Because of cascade production, most of them have been changed into $e^{\pm}$ pairs. Although

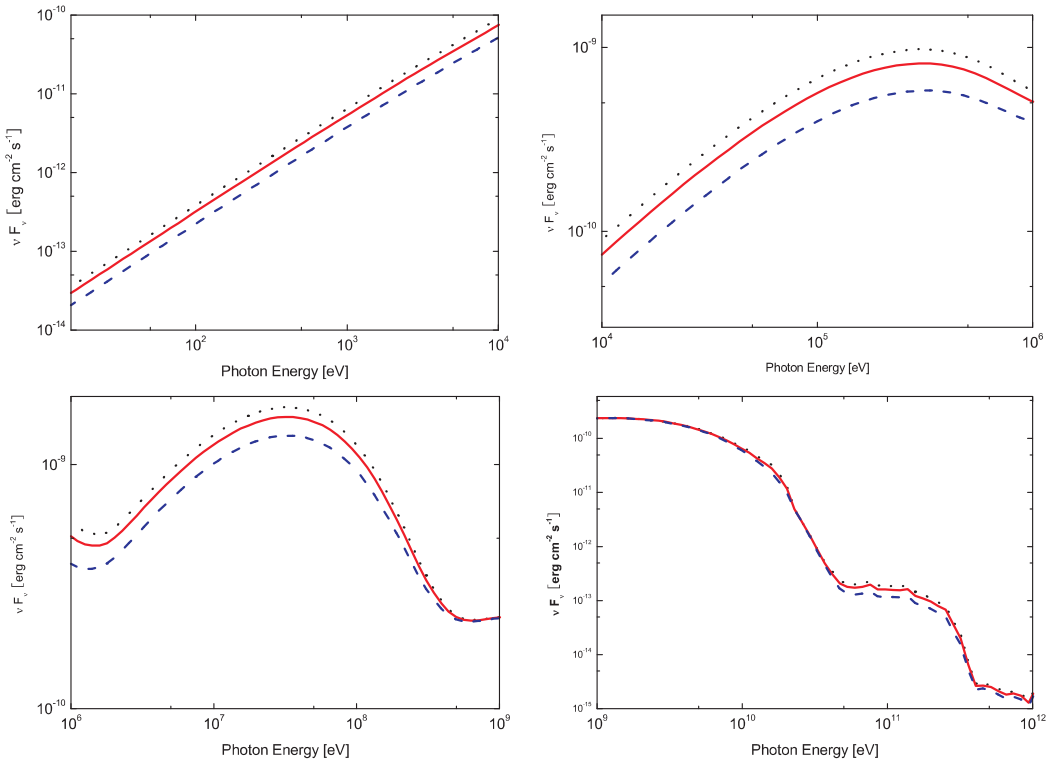

Fig. 4 The predicted spectra at different wavebands corresponding to three different orbital radii (i.e. different phases): 8×10^{11} cm (*dotted line*), 1×10^{12} cm (*solid line*) and 5×10^{12} cm (*dashed line*). An accretion rate of $0.005\ \dot{M}_8$ is used; the other parameters are the same as those of Fig. 3.

there are relatively small numbers of pairs compared to the total number of photons, these pairs are energetic enough to facilitate the following cascades. From this figure, we can see that the second, third and fourth synchrotron emissions dominate emission output ranging from UV to $\sim$ 10 GeV bands. The second and third cases of ICS are dominant at very high energies, but these TeV emissions are too low to provide the needed flux for the current telescopes HESS and MAGIC, nevertheless, they may be detectable by future instruments with higher sensitivity and wider energy ranges, such as the Cherenkov Telescope Array (CTA). On the other hand, the fifth generation of synchrotron and ICS (which cannot be shown in the figure) spectra have become lower, which implies that the next cascade is negligible.

As previously mentioned, the attenuation from stellar photons can bring about orbital modulations of radiation. In Figure 4, we calculate spectral energy distributions at different phases (corresponding to different orbital radii) of an elliptical orbit: 8×10^{11} cm (dotted line), 1×10^{12} cm (solid line) and 5×10^{12} cm (dashed line). For clarity, we have split the whole broadband spectrum into four bands. As shown in this figure, the orbital modulation of emissions is evident, ranging from visible to TeV bands except for a weak GeV modulation.

4 APPLICATION TO LS I + 61° 303

In this section, we apply the magnetospheric emission model to LS I + 61° 303. This source is a high-mass X-ray binary system with a circumstellar disk located at a distance of $\sim$ 2 kpc (Frail

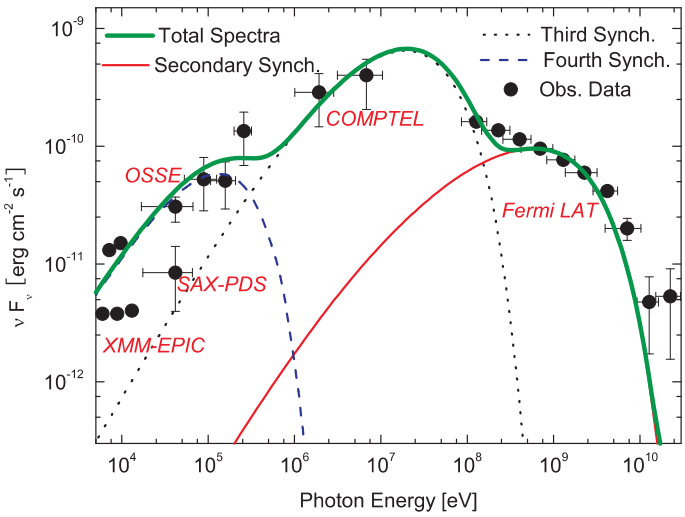

Fig. 5 Fitting the emission spectra of LS I + 61° 303. The fitting parameters are the accretion rate of $0.01\ \dot{M}_8$, effective factor of $\eta = 0.03$, magnetic field of the pulsar's surface of $10\ B_{12}$, orbital distance of 8.6×10^{11}cm at periastron, pulsar mass of $1.4\ M_\odot$ and spectral index of 2.5. The plotted observations are: OSSE data from Strickman et al. (1998), XMM-EPIC and SAX-PDS data from Sidoli et al. (2006), COMPTEL data from van Dijk et al. (1996) and *Fermi* data from Abdo et al. (2009a).

& Hjellming 1991), a 26.496-day orbital period (Taylor & Gregory 1982) and an eccentric orbit of $e = 0.55 - 0.72$ (Casares et al. 2005). The companion star has a mass of $12\ M_\odot$, an effective surface temperature of 2.25×10^4 K and a radius of $13.4\ R_\odot$ (Casares et al. 2005). The temperature of the circumstellar disk is 1.75×10^4 K (Marti & Paredes 1995), which is valid in the inner region of the stellar disk. For this reason, we consider r (see Eq. (12)) to be an orbital radius at periastron passage where the given value for temperature is reliable (Christiansen et al. 2006). However, significant uncertainty still exists in the mass of the central compact star. The radial velocity of the companion star is consistent with a $1.4\ M_\odot$ NS. However, if the orbital inclination is $\leq 25°$, this corresponds to a $\geq 3\ M_\odot$ black hole (Casares et al. 2005).

Recently, *Fermi* LAT has detected the emission and light curve of a source (Abdo et al. 2009a) at high energy γ-ray bands (20 MeV – 100 GeV). The light curve is depicted by a broad peak after periastron, and a smaller peak just before apastron. The emission spectrum is best fitted by a power law plus an exponential cutoff, with a photon index of 2.21 and a cutoff energy of $\sim$ 6.3 GeV. However no considerable spectral change with orbital phase has been detected. On the other hand, MAGIC (Albert et al. 2006) has reported very high-energy γ-ray emissions which show a peak flux close to apastron. Hence, emission signatures between high energies and very high-energies imply the existence of an anti-correlation.

Bednarek (2009b) proposed an accreting magnetar model to study the emission spectral distribution of LS I + 61° 303, by assuming the central compact object is an NS of the magnetar type. Very recently, a magnetar-like signal has been detected by Torres et al. (2012), however, further identification is needed. Therefore, in our fitting of LS I + 61° 303, a high magnetic field of $10\ B_{12}$ is used. On the other hand, because the thermal X-ray emission has still not been detected, we use a small accretion rate $0.01\ \dot{M}_8$ which corresponds to a low thermal X-ray flux.

In Figure 5, we present the fitting results from LS I + 61° 303 at periastron. The fitting parameter is shown in the caption of the figure. The second, third and fourth generations of synchrotron processes dominate emissions ranging from hard X-rays to high-energy γ-rays. Other radiation spectra (similar to those in Fig. 3) are negligible and are not plotted on the figure. As shown in the figure, the fourth synchrotron emission is dominant in the X-ray domain and the third synchrotron emission contributes emission flux at soft γ-ray bands ($\sim$ 1–100 MeV). The *Fermi* LAT observations can be reproduced by the second and third synchrotron emissions. The theoretical spectra can reproduce the observations ranging from hard X-ray to γ-ray bands. Meanwhile, this spectrum shows a cutoff at $\sim$ GeV and can explain the cutoff spectral features detected by *Fermi* LAT.

Nevertheless, we would like to discuss two aspects of observational fittings. Firstly, the spectral energy distributions systematically underestimate the observed data points at energies >5 GeV in Figure 5 (i.e. the last three data points at the high energy end from *Fermi* LAT). If we adjust the related parameters to fit the last three data points, the other *Fermi* LAT data points at lower energies would not be fitted well. In order to fit the last three data points, some additional mechanisms are required. Here, we present a possibility. In the framework of the magnetospheric gap model, both electrons and protons can be accelerated in the gap in the opposite direction. As a first step, we only focus on the lepton processes in this work. If hadron interactions, i.e., proton-proton ($p - p$) collisions, are considered, interactions between the accelerated high energy protons and cold protons from the stellar companion or disk wind can also excite electromagnetic cascades. Furthermore, the secondary electron-positron pairs from $p - p$ interactions can produce synchrotron emissions, which will be expected to remedy the current discrepancy. Secondly, the currently theoretical spectra at the TeV bands are very low, compared with the very high energy data of LS + 61° 303 (e.g., Albert et al. 2006). Thus we do not plot data points from the TeV band. If the $p - p$ interactions are included, we expect γ-ray emissions from the π^0 meson decay can reproduce the very high energy observations.

In conclusion, the *Fermi* LAT observation of LS I + 61° 303 should arise from the magnetosphere region of the pulsar. Due to the fact that a gap formation needs the angular velocity $\Omega_{\rm d}$ of the inner accretion disk to be larger than the pulsar value Ω, we can infer from this limit that the pulsar may be an old, slowly spinning NS.

5 DISCUSSION AND SUMMARY

Based on the direct electric field acceleration model from an accreting X-ray binary pulsar (Cheng & Ruderman 1989, 1991), we consider three photon fields from the polar cap, accretion disk and massive companion star with a circumstellar disk. These photons permeate the gap, shield the accelerated particles and excite the cascade of emissions. We numerically carry out the cascade processes of emissions up to the fifth generation of emissions. Furthermore, we apply this magnetospheric emission model to fit observations of LS I + 61° 303. We have found that the second, third and fourth generations of synchrotron dominate emissions ranging from hard X-ray to γ-ray wavelengths. We show that the theoretical spectra can reproduce observations at hard X-rays and γ-rays. It is important that our results can explain the cutoff features at a few GeV. Hence we propose that the emission signatures from LS I + 61° 303, reported by *Fermi*, should originate from the magnetosphere region of the pulsar. This source of emission may be a common phenomenon in this class of sources. The model should explain spectral variabilities due to the orbital periodicity (also see Fig. 4), although at this stage we do not simulate the spectral changes of LS I + 61° 303 from different accretion rates or soft photon densities. Moreover, what physical mechanism results in the observed long-term variability in X-ray and γ-ray is not yet clear, which will be left for future work.

Regarding the acceleration mechanism in an accreting X-ray binary, some studies regard the acceleration region as being located in the region with Alfvén disturbance (e.g., Bednarek 2009a). In this model, the dense wind of a companion star can be partially captured by a central NS, and

the spherically accreted matter can penetrate the inner magnetosphere of the compact star. With accretion, the balance between magnetic pressure and pressure inserted by accreted matter grows progressively more unstable, and thus a turbulent, magnetized shock region can be formed. This shock region can provide a condition for acceleration of particles to relativistic energies. Nevertheless their studies focus on a spherical accretion structure rather than a disk accretion scenario, and still do not consider the geometrical structure of particle acceleration by the *Fermi* shock mechanism in detail.

On the other hand, some studies suggest that the violent magnetic reconnection in a jet/accretion disk system can accelerate particles to relativistic energies, with a power law index that is similar to the *Fermi* shock acceleration processes (de Gouveia dal Pino & Lazarian 2005; de Gouveia Dal Pino et al. 2010). Furthermore, the emission model of magnetospheric charge separation studied in this work can accelerate particles to relativistic energies by the direct acceleration of the electric field in the gap (Cheng & Ruderman 1989, 1991).

In this work, we do not study the geometrical structure of the gap for the accreting X-ray pulsar in detail. We still use the old version of the gap model (also because of the lack of a new version of the gap model), which is a two-dimensional model. For the magnetospheric acceleration mechanism in an isolated pulsar, however, there have been many studies since the outer gap model of Cheng et al. (1986) was published. Zhang & Cheng (1997) proposed a three-dimensional outer gap model to study high-energy emission of an isolated pulsar. Recently, this three-dimensional gap model has been revised to explain the phase-resolved spectrum of the Crab pulsar (e.g., Tang et al. 2008; Zhang & Li 2009); these works argue that the gap can extend below the null charge surface up to ~ 10 radii of the pulsar, and the azimuthal extension of the outer gap can reach $\sim 250^\circ$ from the initial $\sim 180^\circ$. With elicitation from these studies, we think that a detailed study about geometrical structure (including a three-dimensional gap) and acceleration processes of particles is needed in the case of the accreting X-ray pulsar. However it will become more complex than that of an isolated pulsar due to a combination of effects. At that moment, one can study the phase-resolved spectrum with orbital changes in detail.

In addition, the current spectra cannot reproduce the very high-energy observations by telescopes that are operating at present (but are possible for the upcoming CTA); we suggest that the accelerated relativistic protons in the gap can interact with cold protons from a disk and/or with a stellar wind from a high-mass companion, and emit TeV emissions via $p-p$ collisions. Alternatively, these high-energy protons can also emit very high-energy γ-rays by $p-p$ interactions. We expect these emissions can explain the anti-correlation between *Fermi* LAT data and TeV data, the correlation of TeV emissions with the soft X-rays and the orbital modulation of emissions. This will be the direction of future work.

Acknowledgements We appreciate the referee for his/her valuable comments and suggestions that significantly improved our manuscript. This work is partly supported by the Guizhou Provincial Natural Science Foundation (No. 2010080), the Science and Technology Foundation of Guizhou Province (No. LKT[2012]27) and the National Natural Science Foundation of China (Grant No. 11363003).

References

Abdo, A. A., Ackermann, M., Ajello, M., et al. 2009a, ApJ, 701, L123
Abdo, A. A., Ackermann, M., Ajello, M., et al. 2009b, ApJ, 706, L56
Abdo, A. A., Ackermann, M., Ajello, M. et al. 2009, Science, 326, 1512
Abdo, A. A., Ackermann, M., Ajello, M., et al. 2011, ApJ, 736, L11
Ackermann, M., Ajello, M., Ballet, J., Fermi LAT Collaboration 2012, Science, 335, 189
Aharonian, F., Akhperjanian, A. G., Aye, K.-M., et al. 2005a, Science, 309, 746

Aharonian, F., Akhperjanian, A. G., Aye, K.-M., et al. 2005b, A&A, 442, 1
Aharonian, F. A., Akhperjanian, A. G., Bazer-Bachi, A. R., et al. 2007, A&A, 469, L1
Albert, J., Aliu, E., Anderhub, H., et al. 2006, Science, 312, 1771
Albert, J., Aliu, E., Anderhub, H., et al. 2007, ApJ, 665, L51
Bednarek, W. 2009a, A&A, 495, 919
Bednarek, W. 2009b, MNRAS, 397, 1420
Blumenthal, G. R., & Gould, R. J. 1970, Reviews of Modern Physics, 42, 237
Bosch-Ramon, V., & Khangulyan, D. 2009, International Journal of Modern Physics D, 18, 347
Casares, J., Ribas, I., Paredes, J. M., Martí, J., & Allende Prieto, C. 2005, MNRAS, 360, 1105
Cheng, K. S., Ho, C., & Ruderman, M. 1986, ApJ, 300, 500
Cheng, K. S., & Ruderman, M. 1989, ApJ, 337, L77
Cheng, K. S., & Ruderman, M. 1991, ApJ, 373, 187
Cheng, K. S., Lau, M. M., Cheung, T., Leung, P. P., & Ding, K. Y. 1992, ApJ, 390, 480
Christiansen, H. R., Orellana, M., & Romero, G. E. 2006, Phys. Rev. D, 73, 063012
de Gouveia dal Pino, E. M., & Lazarian, A. 2005, A&A, 441, 845
de Gouveia Dal Pino, E. M., Piovezan, P. P., & Kadowaki, L. H. S. 2010, A&A, 518, A5
Dubus, G. 2006, A&A, 456, 801
Dubus, G., Cerutti, B., & Henri, G. 2008, A&A, 477, 691
Frail, D. A., & Hjellming, R. M. 1991, AJ, 101, 2126
Frank, J., King, A., & Raine, D. J. 2002, Accretion Power in Astrophysics (edn.3rd; Cambridge: Cambridge Univ. Press)
Harding, A. K., & Preece, R. 1987, ApJ, 319, 939
Hinton, J. A., Skilton, J. L., Funk, S., et al. 2009, ApJ, 690, L101
Jauch, J. M., & Rohrlich, F. 1976, The Theory of Photons and Electrons, The Relativistic Quantum Field Theory of Charged Particles with Spin One-half (New York: Springer)
Kato, S., Fukue, J., & Mineshige, S. 2008, Black-Hole Accretion Disks – Towards a New Paradigm (Kyoto: Kyoto Univ. Press)
Khangulyan, D., Aharonian, F., & Bosch-Ramon, V. 2008, MNRAS, 383, 467
Leung, P. P., Cheng, K. S., & Fung, P. C. W. 1993, ApJ, 410, 309
Lipunov, V. M., Börner, G., & Wadhwa, R. S. 1992, Astrophysics of Neutron Stars (Berlin: Springer-Verlag)
Marti, J., & Paredes, J. M. 1995, A&A, 298, 151
Mirabel, I. F. 2006, Science, 312, 1759
Mirabel, I. F. 2012, Science, 335, 175
Nolan, P. L., Abdo, A. A., Ackermann, M., et al. 2012, ApJS, 199, 31
Paredes, J. M., Bosch-Ramon, V., & Romero, G. E. 2006, A&A, 451, 259
Piano, G., Tavani, M., Vittorini, V., et al. 2012, A&A, 545, A110
Rodriguez, J., & Bodaghee, A. 2008, in AIPC, 1010, A Population Explosion: The Nature & Evolution of X-ray Binaries in Diverse Environments, eds. R. M. Bandyopadhyay, S. Wachter, D. Gelino, & C. R. Gelino, 225
Romero, G. E., Okazaki, A. T., Orellana, M., & Owocki, S. P. 2007, A&A, 474, 15
Shakura, N. I., & Sunyaev, R. A. 1973, A&A, 24, 337
Sidoli, L., Pellizzoni, A., Vercellone, S., et al. 2006, A&A, 459, 901
Strickman, M. S., Tavani, M., Coe, M. J., et al. 1998, ApJ, 497, 419
Tang, A. P. S., Takata, J., Jia, J. J., & Cheng, K. S. 2008, ApJ, 676, 562
Taylor, A. R., & Gregory, P. C. 1982, ApJ, 255, 210
Torres, D. F., Rea, N., Esposito, P., et al. 2012, ApJ, 744, 106
van Dijk, R., Bennett, K., Bloemen, H., et al. 1996, A&A, 315, 485
Yamaguchi, M. S., & Takahara, F. 2010, ApJ, 717, 85
Yamaguchi, M. S., & Takahara, F. 2012, ApJ, 761, 146

Zabalza, V., Paredes, J. M., & Bosch-Ramon, V. 2011, A&A, 527, A9
Zhang, J.-F., Zhang, L., & Fang, J. 2009, PASJ, 61, 949
Zhang, J. F., Feng, Y. G., Lei, M. C., Tang, Y. Y., & Tian, Y. P. 2010, MNRAS, 407, 2468
Zhang, J.-F., Zhu, Y., & Zhang, L. 2011, RAA (Research in Astronomy and Astrophysics), 11, 445
Zhang, J. F., & Feng, Y. G. 2011, MNRAS, 410, 978
Zhang, L., & Cheng, K. S. 1997, ApJ, 487, 370
Zhang, L., & Li, X. 2009, ApJ, 707, L169